Proceedings of IMECE2009
2009 ASME International Mechanical Engineering Congress and Exposition
November 13-19, Lake Buena Vista, Florida, USA

IMECE2009-11926

MODELING THE EFFECT OF FLUID-STRUCTURE INTERACTION ON THE IMPACT DYNAMICS OF PRESSURIZED TANK CARS

Hailing Yu
MacroSys Research and Technology
55 Broadway, Cambridge, MA 02142, USA
Hailing.Yu@dot.gov

Yim H. Tang
Volpe National Transportation Systems Center
55 Broadway, Cambridge, MA 02142, USA
Yim.Tang@dot.gov

Jeffrey E. Gordon
Volpe National Transportation Systems Center
55 Broadway, Cambridge, MA 02142, USA
Jeffrey.Gordon@dot.gov

David Y. Jeong
Volpe National Transportation Systems Center
55 Broadway, Cambridge, MA 02142, USA
David.Jeong@dot.gov

ABSTRACT

This paper presents a computational framework that analyzes the effect of fluid-structure interaction (FSI) on the impact dynamics of pressurized commodity tank cars using the nonlinear dynamic finite element code ABAQUS/Explicit. There exist three distinct phases for a tank car loaded with a liquefied substance: pressurized gas, pressurized liquid and the solid structure. When a tank car comes under dynamic impact with an external object, contact is often concentrated in a small zone with sizes comparable to that of the impacting object. While the majority of the tank car structure undergoes elastic-plastic deformations, materials in the impact zone can experience large plastic deformations and be stretched to a state of failure, resulting in the loss of structural integrity. Moreover, the structural deformation changes the volume that the fluids (gas and liquid) occupy and consequently the fluid pressure, which in turn affects the structural response including the potential initiation and evolution of fracture in the tank car structure.

For an event in which the impact severity is low and the tank car maintains its structural integrity, shell elements following elastic-plastic constitutive relations can be employed for the entire tank car domain. For events in which the impact severity is higher and the tank car is expected to be punctured, an equivalent plastic strain based fracture initiation criterion expressed as a function of stress triaxiality is adopted for the material in the tank car's impact zone. The fracture initiation is implemented for ductile, shear and mixed fracture modes and followed by further material deterioration governed by a strain softening law. Multi-layered solid elements are employed in the impact zone to capture this progressive fracture behavior.

The liquid phase is modeled with a linear U_s–U_p Hugoniot form of the Mie-Grüneisen equation of state, and the gas phase is modeled with the ideal gas equation of state. Small to moderate amounts of fluid sloshing are assumed for an impacted tank car in this study. As such, the FSI problem can be solved with the Lagrangian formulation of ABAQUS, and appropriate contact algorithms are employed to model the multi-phase interactions. The force, displacement and impact energy results from the finite element analysis show good correlations with the available shell (side) impact test data. The puncture energy of a tank car in a shell impact scenario is further analyzed. It is demonstrated that the FSI effect needs to be adequately addressed in an analysis to avoid overestimating the puncture resistance of a tank car in an impact event.

INTRODUCTION

Pressurized commodity tank cars are commonly employed in the railroad industry to transport liquefied goods including hazardous materials (hazmat) such as compressed flammable (e.g., propane) or toxic gases (e.g., chlorine). Severe impacts in some railroad accidents compromised the structural integrity of tank cars, released hazmat into the surrounding environment and caused human fatalities and injuries, environmental damage and economic losses [1-3]. Thus improving the structural integrity of railroad tank cars is of great importance, and it requires improved tank car designs based on a better understanding of the dynamics of individual tank components and their interactions [4]. To achieve these goals,

computational methods such as finite element analysis (FEA) have proven to be a powerful tool that complements experimental approaches.

Under normal operating conditions, both liquid and vapor forms of a substance being transported coexist in a tank car. The pressure of a gaseous vapor in dynamic equilibrium with its liquid form at a given temperature is called vapor pressure. For instance, the Antoine equation calculates the vapor pressure as follows

$$\ln(P)=A-B/(T+C) \quad (1)$$

where P is vapor pressure, T is temperature and A, B and C are Antoine coefficients. Figure 1 shows the vapor pressures of water and chlorine over a range of temperatures according to Eq. (1), with the Antoine coefficients obtained from http://www.cheresources.com/data.xls. While vapor pressures of water appear to be negligible at normal temperatures, those of chlorine are more significant. Figure 2 depicts three interacting phases in a tank car loaded with chlorine: solid structure, liquid and gas. The liquid and gas phases are also referred to as fluid phases.

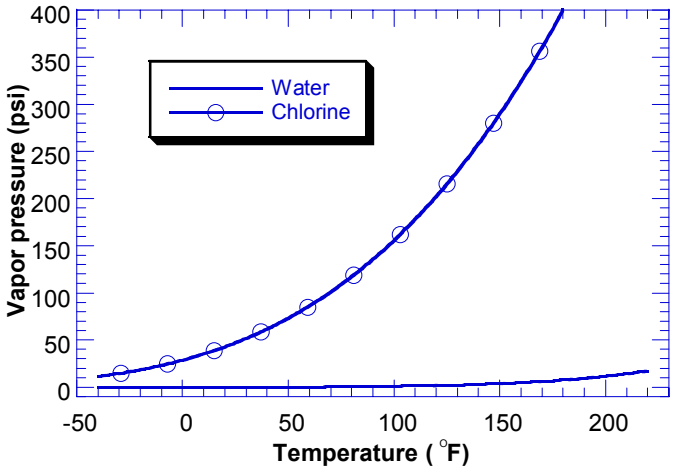

Fig. 1: Vapor pressures of water and chlorine as functions of temperature

A tank car structure responds to external impact loading with elastic-plastic deformations that ultimately can be stretched to a state of failure. In a tank car with liquefied lading such as chlorine, the fluid pressure also transmits forces to the inner wall and balances with the internal forces of the tank container. This is a typical fluid-structure interaction (FSI) phenomenon because the fluid pressure affects the structural deformation and vice versa. Simplified computational approaches have avoided explicitly modeling one or both fluid phases by replacing them with prescribed, constant inner wall pressure and/or lumped fluid mass. A more realistic computational model of a loaded tank car, however, needs to include multiple phases: solid structure, pressurized liquid and pressurized gas.

This paper presents a computational study of the multi-phase interactions in a tank car during a dynamic event using the commercial FEA software ABAQUS. Provided that the degree of fluid sloshing is small to moderate, the FSI problem can be solved within the ABAQUS Lagrangian framework. The paper is organized as follows. First, shell (or side) impact tests on full scale tank cars are described. Second, a computational multi-phase approach is presented. Third, the computational method is applied to simulate the FSI effects in the shell impact tests, and the simulation results are verified with the experimental data. Fourth, tank car puncture is predicted with the multi-phase FEA framework. Last, conclusions are drawn from the study, and additional applications of the method are discussed.

EXPERIMENTAL STUDY

The main structure of a tank car consists of two ellipsoidal ends (or heads) connected by a cylindrical shell. An object hits anywhere on the shell in a shell impact scenario, and it hits anywhere on the heads in a head impact scenario. Head impact tests on full-scale tank cars were conducted in as early as the 1970's [5] and then during the 1990's [6-7], whereas head component tests were done more recently. In 2007, full-scale shell impact tests were conducted at the Transportation Technology Center in Pueblo, Colorado. These tests were mainly aimed at evaluating the crashworthiness performance of existing tank cars. Moreover, the test data can help to develop

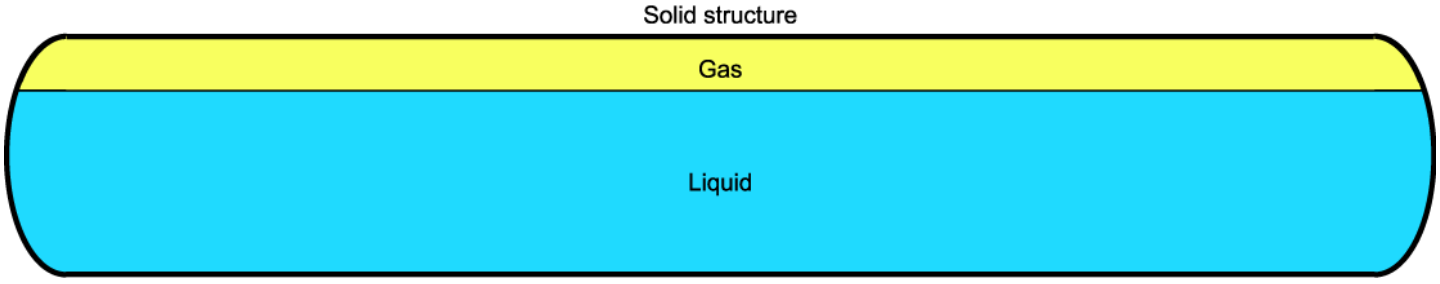

Fig. 2: Illustration of solid, liquid and gas phases comprising a loaded tank car

Fig. 3: Tank and ram cars in a shell impact test

and verify computational models [8].

Figure 3 shows typical tank and ram cars used in the shell impact tests in Pueblo, Colorado. For obvious safety reasons the tank car was filled with water in lieu of liquid chlorine, to 89.4% of its capacity (i.e., 10.6% outage). In addition, clay slurry was added in the water, and the mixture had the approximate density of liquid chlorine. Air occupied the rest of the tank volume and was pressurized initially to 100 psi to simulate the condition in a tank car loaded with liquid chlorine. The tank car assembly weighed about 263,000 pounds with its liquid content, a steel jacket and other accessories. It was placed with one side against a concrete wall and the other side exposed to impact from the ram car. The ram car was a ballasted flatcar that weighed 286,000 pounds and had a protruding beam to which an impactor was attached. Two impactors were employed in the shell impact tests, and their surface geometries are illustrated in Fig. 4. Impactor I had a 17″x23″ face (approximately the size of a draft sill cross-section) whose edges were rounded with 1″ radius, and Impactor II had a smaller, 6″x6″ face (approximately the size of a coupler shank cross-section) whose edges were rounded with 0.5″ radius.

Accelerometers on the ram car yielded data to calculate impact forces and impactor displacements. Displacement transducers were mounted on the interior tank wall, providing tank indentation data. Pressure transducers were also placed on the interior tank wall to monitor the liquid pressure at selected locations. No data channel was available for monitoring the air pressure.

An assurance test was first conducted with limited instrumentation, followed by two fully instrumented tests (Test 1 and Test 2). Impactor I was employed in Test 1 and Impactor II in Test 2. In both tests, the ram car ran the impactor perpendicularly to the center of the tank shell (at 14 mph in Test 1 and 15.1 mph in Test 2). The tank car was dented a maximum 26 inches but maintained its structural integrity in Test 1. The tank car was punctured and the fluids escaped in Test 2. The peak force reached about 1290 kips in Test 1 and nearly 900 kips in Test 2.

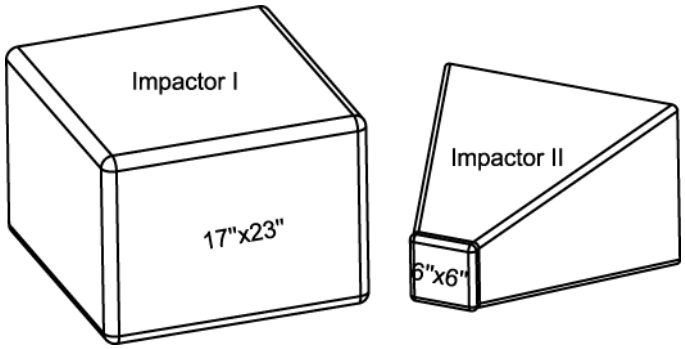

Fig. 4: Schematic of Impactor surfaces

THREE-PHASE FINITE ELEMENT MODEL

Finite element models were developed to simulate the tests described above. In one simplified approach, the gas phase was omitted, and the fluid pressure was replaced with a prescribed, constant pressure on the inner wall of the tank container. This approach can be fairly accurate when the structural deformation is small or localized and thus has a minimal effect on the fluid pressure. However, in the shell impact cases described above, the structural deformation spanned a large domain, the FSI effect was sufficiently strong, and the simplified approach became inaccurate. In the computational framework presented here, all of the solid, liquid and gas phases following different sets of governing equations were explicitly modeled, and their interactions were accounted for via available contact options.

Governing equations

Solid structure

The tank car structure is made of specialty steel such as TC-128B. The behavior of this solid structure phase is modeled with elastic-plastic and fracture constitutive relations. The elastic behavior is assumed to be linear and isotropic with Young's modulus E and Poisson's ratio ν. Once the elastic limit is reached, a modified Ramberg-Osgood strain hardening law [9] is followed

$$\varepsilon = \sigma/E + (\sigma/K)^n \tag{2}$$

where ε and σ are true strain and true stress, respectively, and n and K are material constants determined from basic material parameters such as the initial yield strength σ_{y0}.

As the yield stress evolves to its peak level, fracture or damage is assumed to initiate at an equivalent plastic strain $\bar{\varepsilon}^{pl} = \bar{\varepsilon}_0^{pl}$, which can be a function of stress triaxiality, strain rate, temperature, etc. This study adopts a fracture initiation criterion dependent on the stress triaxiality η, which is defined as the ratio of the hydrostatic mean stress (σ_m) to the von Mises equivalent stress ($\bar{\sigma}$)

$$\eta = \sigma_m/\bar{\sigma} \tag{3}$$

where

$$\sigma_m = \frac{1}{3}(\sigma_1 + \sigma_2 + \sigma_3) \tag{4}$$

and

$$\bar{\sigma} = \sqrt{\frac{1}{2}\left[(\sigma_1 - \sigma_2)^2 + (\sigma_2 - \sigma_3)^2 + (\sigma_3 - \sigma_1)^2\right]} \tag{5}$$

A fracture locus can be constructed in the $(\eta, \bar{\varepsilon}_0^{pl})$ plane from a material's fracture initiation criterion. A three-branch fracture locus similar to that calibrated by Lee and Wierzbicki [10] for industrial aluminum and steel is adopted and expressed as

$$\bar{\varepsilon}_0^{pl} = \begin{cases} \infty, & \eta \le -1/3 \\ C_1/(1+3\eta), & -1/3 < \eta \le 0 \\ C_1 + (C_2 - C_1)(\eta/\eta_0)^2, & 0 \le \eta \le \eta_0 \\ C_2\,\eta_0/\eta, & \eta_0 \le \eta \end{cases} \tag{6}$$

where C_1 is $\bar{\varepsilon}_0^{pl}$ in pure shear (η=0), and C_2 is $\bar{\varepsilon}_0^{pl}$ in uniaxial tension where $\eta = \eta_0$=1/3. The fracture locus derived from this expression is plotted in Fig. 5: Branch I for ductile fracture due to the mechanism of void nucleation, growth and coalescence; Branch III for shear fracture due to shear bank localization; and Branch II for mixed mode fracture. Note that the original calibration by Lee and Wierzbicki [10] treated η as the average stress triaxiality over a deformation history; in particular, η_0 for uniaxial tension was assigned values greater than 1/3. However, η_0=1/3 was adopted in this study because (1) previous studies established that 1/3 was a good approximation of the stress triaxiality at the center section of a uniaxial tensile specimen [11], and (2) the stress triaxiality appeared to remain at 1/3 for most of the deformation history obtained for a smooth (i.e., unnotched) tensile specimen [12].

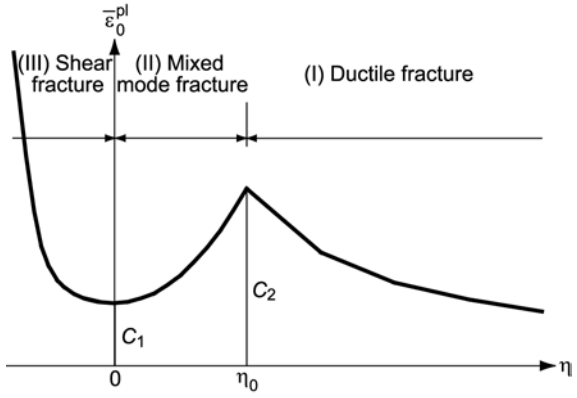

Fig. 5: Three-branch fracture initiation locus for industrial aluminum or steel

ABAQUS' "progressive damage and failure" material model accommodates the material behavior described above [13]. With a predefined fracture initiation criterion $\bar{\varepsilon}_0^{pl} = \bar{\varepsilon}_0^{pl}(\eta)$, ABAQUS determines that damage initiates if the following condition is met

$$\omega_D = \int \frac{d\bar{\varepsilon}^{pl}}{\bar{\varepsilon}_0^{pl}} = 1 \tag{7}$$

where ω_D is a state variable that increases monotonically with plastic deformation. This takes into account the plastic deformation history in determining any fracture initiation. ABAQUS directs this implementation to the ductile fracture type, but a fracture initiation criterion defined over the stress triaxiality range (-∞, +∞) would cover the shear and mixed fracture modes as well.

With the onset of damage, the yield stress softens and the elastic modulus degrades until the equivalent plastic strain reaches its failure limit $\bar{\varepsilon}_f^{pl}$. This damage evolution is monitored by an overall damage variable D which starts at 0 when ω_D reaches 1 and progresses to 1 at complete failure. ABAQUS allows various damage evolution forms and for simplicity, this study adopts a linear softening law. To reduce

the mesh dependency inherent in softening responses, ABAQUS has introduced the concept of an element characteristic length (denoted as L_e) in the constitutive relation. Accordingly, an equivalent plastic displacement $\bar{u}^{pl}$ is defined and evolves according to the following equation

$$\dot{\bar{u}}^{pl} = L_e \, \dot{\bar{\varepsilon}}^{pl} \tag{8}$$

When $\bar{u}^{pl}$ reaches $\bar{u}_f^{pl}$ upon complete failure, elements representing failed material points may be removed. These elastic-plastic-fracture constitutive relations for tank car steels were previously employed in modeling the fracture mechanics of unnotched Charpy specimens [14-15].

The thickness dimension of a tank car is considerably smaller that the other dimensions such as tank diameter and length. Previous studies established that to capture pure elastic-plastic behaviors, a shell element formulation was accurate with a typical element size of about two times the tank thickness [16]. For the progressive damage and failure behavior, the shell element formulation can produce misleading results and therefore, a solid element formulation must be employed. Multiple layers of solid elements through the thickness dimension are needed in this case to accurately capture the progressive deterioration process. However, an all-solid-element model of a tank car is expensive; it is also unnecessary with the solid-to-shell coupling technique available in ABAQUS. That is, the impact zone is modeled with multi-layered solid elements, the rest of the domain is modeled with shell elements, and the two domains are joined via solid-to-shell coupling. Figure 6 illustrates a typical mesh involving both shell and solid elements and solid-to-shell coupling.

Liquid phase

The hydrostatic behavior of the liquid phase is governed by equations of state that determine the pressure p (positive in compression) as a function of the density ρ and the specific energy E_m (internal energy per unit mass)

$$p=f(\rho,E_m) \tag{9}$$

The Mie-Grüneisen equation of state available in ABAQUS/Explicit is linear with respect to energy and can be written in the following form

$$p=f_1(\rho)+f_2(\rho)E_m \tag{10}$$

where $f_1(\rho)$ and $f_2(\rho)$ are model-dependent functions of density. A linear U_s–U_p Hugoniot form of the Mie-Grüneisen equation of state is verified to be an effective method to model the behavior of liquids such as water [17]. For this model, the initial density ρ_0 and wave speed c_0 (from which $\rho_0 c_0^2$ yields the elastic bulk modulus) are required material inputs.

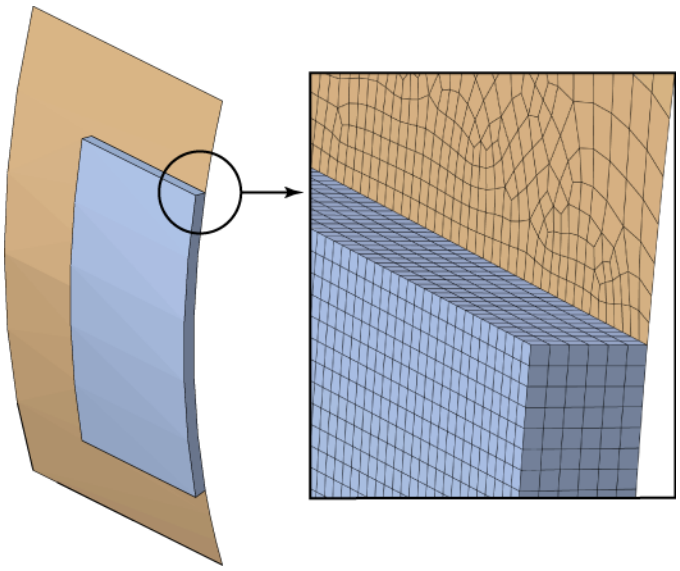

Fig. 6: Typical finite element mesh involving both shell and solid elements in a tank car impact zone

The deviatoric behavior of the liquid phase is assumed to be uncoupled from its volumetric response and governed by either a linear isotropic elastic model or a Newtonian viscous fluid model. The shear viscosity parameter serves as a penalty to suppress the shear modes that can distort a mesh, and it must be small for water which is inviscid.

Gas phase

The gas phase is assumed to follow the ideal gas equation of state

$$pV=mRT \tag{11}$$

where p is the absolute pressure, V is the volume, m is the mass, R is the (specific) gas constant and T is the absolute temperature. The gas constant R is a required input for this model. The ideal gas assumption is approximately true for the conditions considered. If there is no leakage or temperature change, the gas pressure is inversely proportional to the volume that the gas occupies, which can change with structural deformations. It is assumed that the liquid and gas phases are in dynamic equilibrium and that temperature is constant throughout the process.

Modeling fluid-structure interaction

In the experimental study described in a previous section, only small to moderate fluid sloshing was believed to have occurred, and the same was assumed in the modeling approach. Under this assumption, mesh distortion due to fluid flow was moderate at most, and the Lagrangian framework was applied.

In addition to each individual phase, the interactions among different phases needed to be addressed. These

Tab. 1: Material and geometry data and initial condition of tank cars in the tests

Tank material	Inner diameter (inch)	Head thickness (inch.)	Shell thickness (inch.)	Shell length (inch.)	Jacket material	Jacket thickness (inch.)	Initial fluid pressure (psi)
TC-128B	100.75	0.828	0.777	471.47	ASTM A1011/A569	0.119	100

Tab. 2: Model parameters for tank car materials

Material	ρ (lbm-in^{-3})	E (ksi)	ν	σ_{y0} (ksi)	n	K (ksi)	C_1	C_2	$\bar{u}_f^{pl}$ (inch)
TC-128B from Test 1	0.2835	29800	0.3	55	10.55	99.15	-	-	-
TC-128B from Test 2	0.2835	31650	0.3	55	11.17	96.04	0.31	1.05	0.32
ASTM A1011/A569	0.2835	29000	0.3	30	9.00	59.85	0.31	0.92	0.25

interactions were analyzed as inter-phase contacts. The general contact option provides a robust solution to modeling solid-to-liquid contacts. However, contacts involving the gas phase can be more problematic because its mass is extremely small compared to those of the other phases.

The gas-to-liquid interface was usually modeled with no separation, no slip contact, equivalent to firmly attaching two materials along their interface. Alternatively, such contact can be replaced with shared nodes along the interface to achieve the same modeling effect while eliminating a potential source of numerical instability – contacts between two materials vastly mismatched in mass. The choice of either option depended on the application and the desired performance.

To model the gas-to-solid interaction, general contact worked well when the structural model included only shell elements. However, when solid-to-shell coupling was involved, numerous trials led to the conclusion that contact between gas and solid phases must also be specifically defined. In addition, it was helpful to define smooth contact surfaces for the fluids and zero contact thickness for shell elements. Frictionless contact was assumed for all fluid-to-fluid and fluid-to-structure interfaces.

VERIFICATION WITH EXPERIMENTAL DATA

The next step was to simulate the full-scale shell impact tests within the multi-phase FEA framework described above and verify the computational results with the corresponding experimental data. An example problem derived from the shell impact simulations was also analyzed with both the multi-phase approach and a simplified approach where the gas phase was omitted and the fluid pressure was replaced with a constant inner wall pressure. A comparison of the results from both approaches demonstrated that the multi-phase approach accounted for the FSI effect more adequately. The example problem, its analysis and the results are presented in the Appendix. This section compares FEA results from both the multi-phase and simplified approaches with the full-scale shell impact test data.

The material and geometry data of the tank cars involved in the tests and the initial fluid pressure are summarized in Tab. 1. Like its physical counterpart, the tank car model consisted of a cylindrical shell with two ellipsoidal heads. The only other explicitly modeled structural entity was the jacket with a clearance of about four inches from the exterior tank body. All the accessories were lumped into point masses. The model parameters for the steel materials are summarized in Tab. 2. The ram car was modeled as one of the impactor shapes shown in Fig. 4 with a lumped mass of 286,000 pounds. As in the tests, the tank car model was filled with liquid for 89.4% of its volume and gas for 10.6% of its volume. The model parameters for liquid and gas phases are shown in Tab. 3. The liquid properties were derived from those of the clay slurry-water mixture and liquid chlorine, and the gas properties were those of air.

Tab. 3: Model parameters for liquid and gas phases

Material	ρ_0 (lbm-in^{-3})	c_0 (in-sec^{-1})	R (in^2-sec^{-2}-K^{-1})
Liquid	0.0510	34732.95	-
Gas	0.0003	-	479034.86

The initial fluid pressure p_0 was introduced as an initial hydrostatic stress state ($\sigma_{11}=\sigma_{22}=\sigma_{33}=-p_0$, $\sigma_{12}=\sigma_{23}=\sigma_{31}=0$) for the three-dimensional fluid elements. Because initial gaps existed in FE models between the inner tank wall and the fluid surfaces, the fluids would experience an initial volume expansion to close the gaps, which would cause an initial drop in the fluid pressure. To mitigate this effect, a fluid pressure slightly larger than p_0 needed to be assigned for model initialization and was denoted as p_0'. The magnitude of p_0' depends on the model setup and can be determined from iterative initialization steps.

Elastic-plastic and FSI analysis

To simulate shell impact Test 1, only shell elements and elastic-plastic material models were employed, because the deformation was not too severe and the structural integrity was maintained as a result of the impact. Modeling FSI was straightforward with one general contact definition. The calculated mass of the tank car assembly was 268,656 pounds,

within 2.2% of the nominal 263,000 pounds. The problem domain, boundary conditions and loading were assumed to be symmetric about the center transverse section, so the half-symmetric model illustrated in Fig. 7 was developed. In addition to the tank car and its fluid contents, Fig. 7 shows a rigid wall (fixed in space) and a rigid lower support which was attached to the tank car assembly and prevented it from moving downward by means of contract with a fixed rigid floor not shown in the picture. Initially, the impact mass moved at a speed of 14 mph toward the stationary tank assembly. The fluid pressure p_0' for model initialization was 101 psi in this case.

The following analysis results from both the multi-phase and simplified approaches were compared with the experimental data: time histories of the impact force (F, Fig. 8a) and impactor displacement (d, Fig. 8b) along the impact direction; F-d cross plot (Fig. 8c); and time history of the work done by the impact force, or integration of the F-d curve (W, Fig. 8d). The multi-phase FEA results show good correlations with the experimental data. The simplified FEA appeared to underestimate the peak forces and overestimate the rebounding impactor displacements.

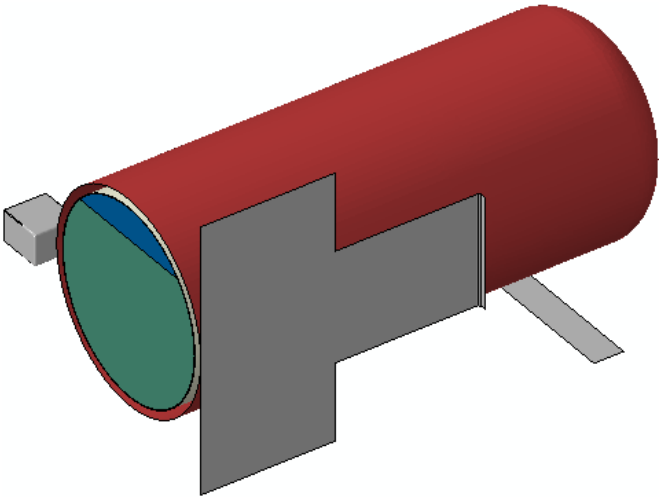

Fig. 7: Half symmetric model for shell impact Test 1

Some key deformation/contact states observed from the simulation were (all times were approximate): the impactor initially contacted the jacket at 0.014 seconds; the jacket overcame the four inch clearance and contacted the exterior tank surface, and the force reached its first peak at 0.124 seconds; the tank surface on the back side contacted the rigid wall at 0.172 seconds, and the force started to climb again; the

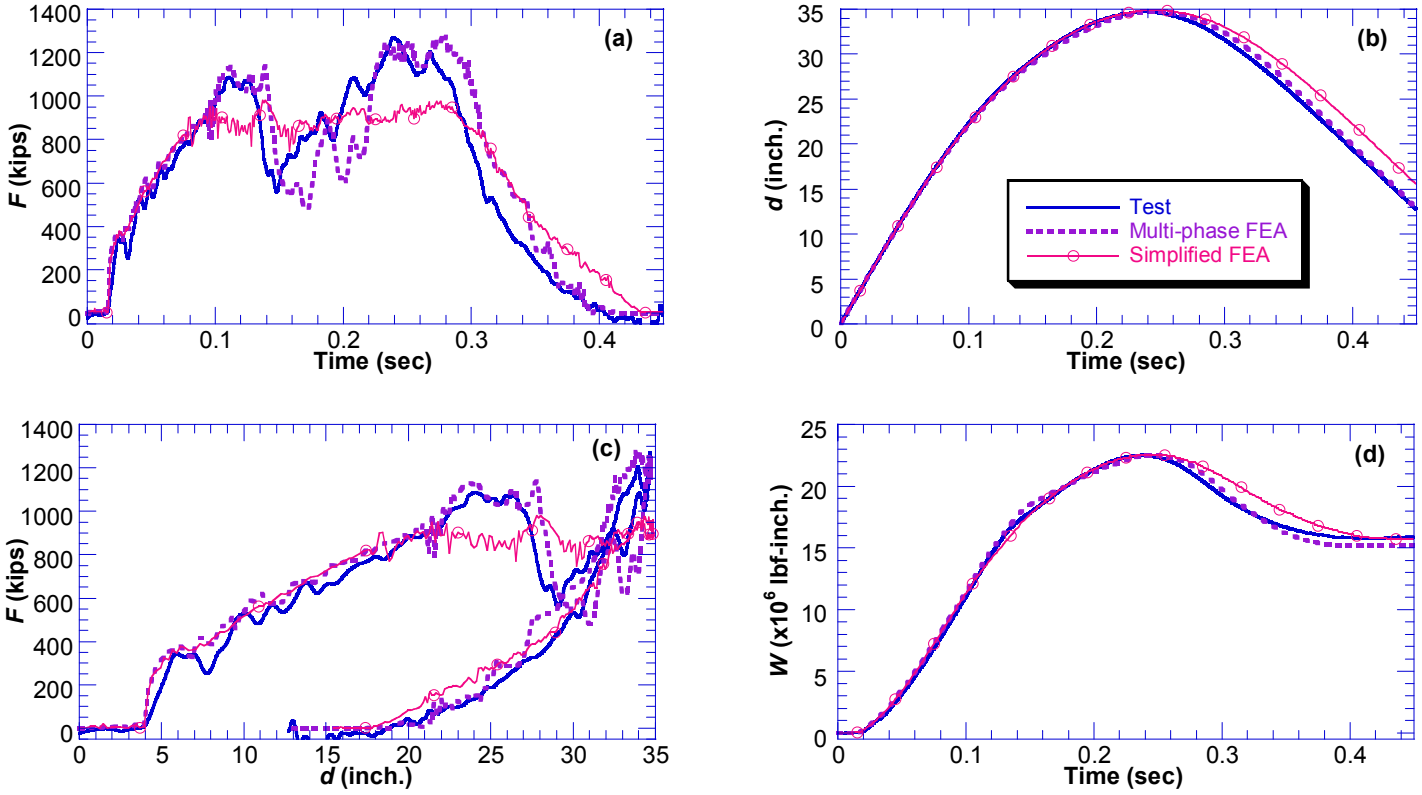

Fig. 8: Test vs. multi-phased and simplified FEA results for shell impact Test 1: (a) impact force F, (b) impactor displacement d, (c) F-d cross plot, and (d) work W done by impact force

maximum tank indentation was reached at approximately the same time as the second peak force at 0.246 seconds, and the impact mass lost its forward momentum and started to rebound from the tank assembly, which in turn rebounded from the rigid wall; at 0.44 seconds, the rebound process was completed and the solid entities were separated from each other.

Fracture and FSI analysis

With a smaller impactor (Impactor II in Fig. 4) and a greater initial impact velocity (15.1 mph), the tank car was punctured in shell impact Test 2. The progressive damage and failure material model was applied to the solid elements in the tank car's impact zone. The tank car assembly weighed 264,756 pounds in the model (the weight difference from that in Test 1 simulation was attributed mainly to differences in the fluid mesh). In addition to the general contact definition, contact interaction was specifically defined for the solid-to-gas interaction. The initialization fluid pressure p_0' was 110 psi for this model, again attributable to the fluid mesh. Figure 9 shows the final damage profile from Test 2 and the model predicted damage at 0.104 seconds. Note that the elastic deformations of the model specimen in Fig. 9 were not recovered, and as a result, the cutout model specimen had a concave shape instead of the convex shape observed in the test specimen. The simulation was discontinued beyond the point of puncture, because the failed structure could no longer contain the fluids.

Figures 10(a-d) show the predicted impact force F, impactor displacement d, F-d cross plot and work W done by the impact force in comparison with the corresponding test data. Again good correlations with the experimental data were observed with the multi-phase approach. The sudden drop in force near 0.1 seconds indicates the breach of the tank car. The multi-phase FEA predicted well both the timing of this event and the maximum force level, whereas the simplified approach under-predicted the peak force and the impactor displacement at puncture.

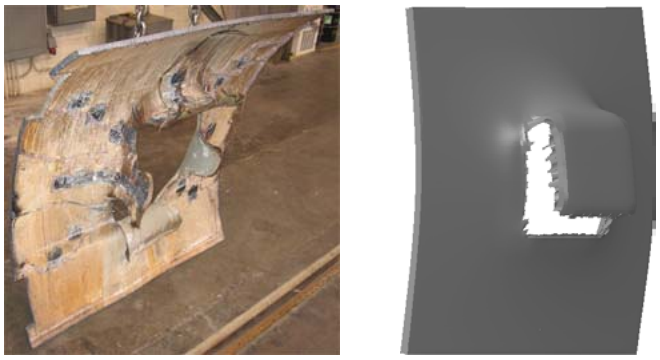

Fig. 9: Damage profile from shell impact Test 2 and model predicted damage at 0.104 seconds

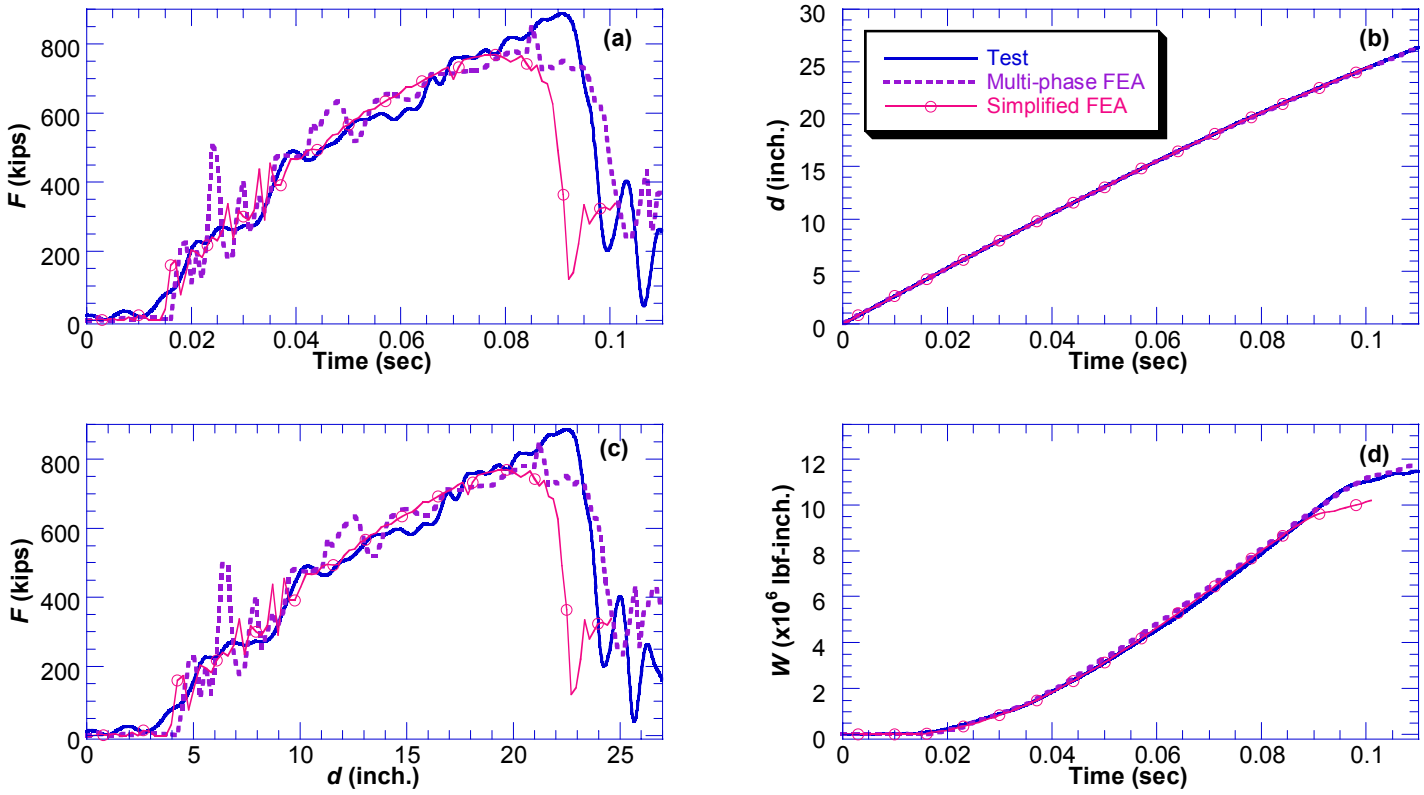

Fig. 10: Test vs. multi-phased and simplified FEA results for shell impact Test 2: (a) impact force F, (b) impactor displacement d, (c) F-d cross plot, and (d) work W done by impact force

AVERAGE GAS PRESSURE

From the multi-phase simulations, the pressure time history averaged over all gas elements, denoted as p_{gas}, can be obtained from ABAQUS. Figure 11 shows the time history of p_{gas} obtained from the simulations of both Tests 1 and 2. The corresponding test data were unavailable. The gas pressure reached a maximum of 135 psi at about 0.216 seconds in the simulation of Test 1, and it reached a maximum of 110 psi right before the tank car punctured in the simulation of Test 2. The maximum air pressure level was higher in Test 1 than in Test 2 because (1) the impact event was more prolonged in Test 1 resulting in more tank deformation and (2) the larger impactor affected broader areas on the tank car and introduced more significant volumetric changes to the fluids. Based on these pressure levels, it appeared that FSI played a stronger role in Test 1 than in Test 2.

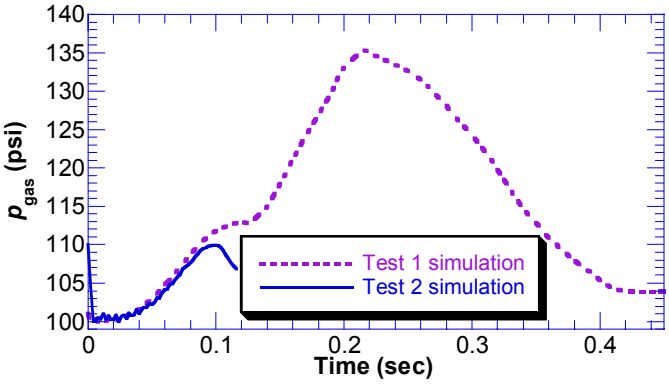

Fig. 11: Average gas pressure p_{gas} obtained from multi-phase simulations of Tests 1 and 2

PUNCTURE ANALYSIS

The puncture energy (E_p) of a tank car can be defined as the minimum impact energy to cause the loss of structural integrity with given tank car configuration, ram car mass, impactor geometry and size, etc. In the simulations, a tank car was deemed to lose its structural integrity when complete, through-the-thickness element failure occurred at any location in the impact zone. The test, simplified FEA and multi-phase FEA showed that the tank car was punctured with an initial impact velocity v_0=15.1 mph under the Test 2 configurations. Further, v_0 was decreased in simulations until the model no longer predicted tank car puncture for a given v_0. Because it was not possible to change v_0 continuously, integer v_0 values were used with decrements of 1 mph. The lowest integer v_0 that did cause puncture was approximated as the minimum puncture velocity of a tank car and denoted as v_p. The puncture energy E_p was estimated as the work done by the impact force up to the point of loss of structural integrity with an initial impact velocity v_0=v_p.

Following the method outlined above, the simplified approach predicted v_p=11 mph and E_p=1.158 million lbf-ft, whereas the multi-phase approach predicted v_p=10 mph and E_p=0.967 million lbf-ft, for the tank car subjected to the configurations of Test 2. Figure 12 shows the *F-d* and *W-d* relations obtained from both the simplified and multi-phase FEA with v_0=v_p. All curves are shown to the point of loss of structural integrity. Compared to the multi-phase approach, the simplified approach overestimated the puncture energy by nearly 20%.

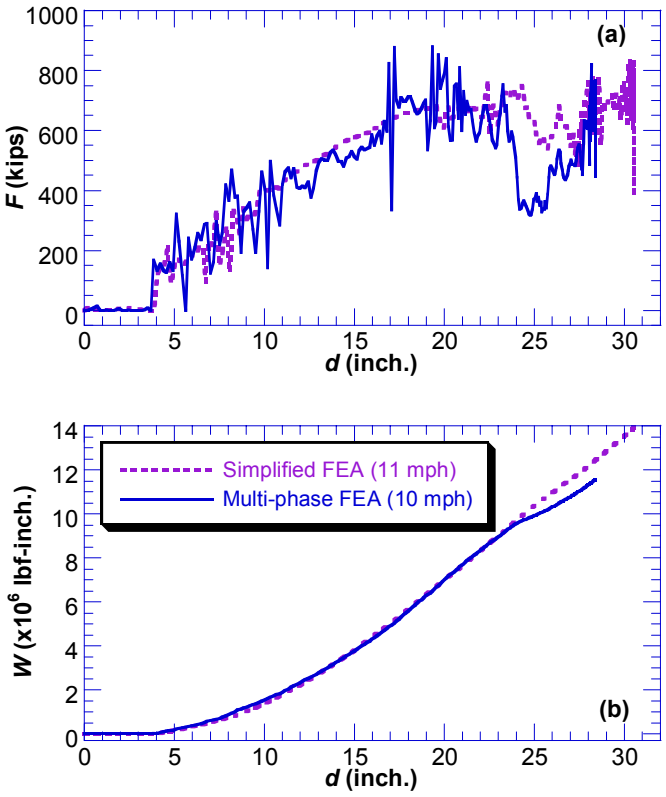

Fig. 12: (a) *F-d* and (b) *W-d* relations obtained from simplified and multi-phase FEA with the predicted minimum puncture velocities as the initial impact velocities under Test 2 configurations

CONCLUSIONS AND DISCUSSIONS

A computational method within the Lagrangian framework of ABAQUS/Explicit was developed and applied in simulating two shell impact tests on full-scale tank cars. The simulations predicted force, displacement and work time histories in good agreement with those recorded in the tests. It was demonstrated that the presented multi-phase modeling approach was effective and accurate in depicting the elastic-plastic-fracture material behavior and fluid-structure interaction mechanisms involved in an impacted tank car.

Although the computational method was verified with shell impact scenarios, it can be similarly applied to head impact scenarios as long as fluid flow does not cause excessive mesh distortion. In addition, the computational approach can

help to evaluate the benefits of improved protective strategies for tank cars.

Potential future work includes incorporating the temperature and strain rate dependencies in the elastic-plastic-fracture constitutive relations of the solid phase. Further, the current method needs to be extended to solve problems involving more significant fluid sloshing.

ACKNOWLEDGMENTS

The Federal Railroad Administration's Office of Research and Development sponsored the research presented in this paper. Mr. Francisco Gonzalez is the FRA project manager for research on railroad tank cars. Mr. Eloy Martinez also provides technical direction to the project. The full-scale shell impact tests described in this paper were funded and conducted by the Next Generation Rail Tank Car Project which was sponsored by Dow Chemical Company, Union Pacific Railroad, and Union Tank Car Company. FRA participated in this project through a Memorandum of Cooperation. HY was employed with Chenega Advanced Solutions and Engineering, LLC during part of this research.

REFERENCES

[1] National Transportation Safety Board (NTSB), "Derailment of Canadian Pacific Railway Freight Train 292-16 and Subsequent Release of Anhydrous Ammonia Near Minot, North Dakota January 18, 2002," Railroad Accident Report NTSB/RAR-04/01, March 2004.

[2] National Transportation Safety Board (NTSB), "Collision of Norfolk Southern Freight Train 192 With Standing Norfolk Southern Local Train P22 With Subsequent Hazardous Materials Release at Graniteville, South Carolina January 6, 2005," Railroad Accident Report NTSB/RAR-05/04, November 2005.

[3] National Transportation Safety Board (NTSB), "Collision of Union Pacific Railroad Train MHOTU-23 With BNSF Railway Company Train MEAP-TUL-126-D With Subsequent Derailment and Hazardous Materials Release, Macdona, Texas, June 28, 2004," Railroad Accident Report NTSB/RAR-06/03, July 2006.

[4] Tyrell, D.C., Jeong, D.Y., Jacobsen, K., Martinez, E., "Improved Tank Car Safety Research," Proceedings of the 2007 ASME Rail Transportation Division Fall Technical Conference, RTDF2007-46013, September 2007.

[5] Phillips, E.A., and L. Olsen, "Final Phase 05 Report on Tank Car Head Study," RPI-AAR Tank Car Safety Research and Test Project, Report RA-05-1-17, 1972.

[6] Coltman, M., and M. Hazel, "Chlorine Tank Car Puncture Resistance Evaluation," Final Report, DOT/FRA/ORD-92/11, 1992.

[7] Larson, W.G., "Aluminum/Cold Temperature Tank Car Puncture Resistance Tests: Data Report," Final Report, DOT/FRA/ORD-92/29, 1992.

[8] Tang, Y.H., Yu, H., Gordon, J.E., Priante, M., Jeong, D.Y., Tyrell, D.C., Perlman, A.B., "Analysis of Full-Scale Tank Car Shell Impact Tests," Proceedings of the 2007 ASME Rail Transportation Division Fall Technical Conference, RTDF2007-46010, September 2007.

[9] Ramberg, W., and W.R. Osgood, "Description of Stress-Strain Curves by Three Parameters," National Advisory Committee for Aeronautics, Technical Note No. 902, 1943.

[10] Lee, Y.-W., and T. Wierzbicki, "Quick Fracture Calibration for Industrial Use," Impact & Crashworthiness Laboratory, Massachusetts Institute of Technology, Report No: 115, August 2004.

[11] Earl, J.C., and Brown, D.K., "Distribution of Stress and Plastic Strain in Circumferentially Notched Tension Specimens," Engineering Fracture Mechanics, 8:599–611, 1976.

[12] Bao, Y., and Wierzbicki, T., "On Fracture Locus in the Equivalent Strain and Stress Triaxiality Space," International Journal of Mechanical Sciences, 46:81-98, 2004.

[13] ABAQUS Analysis User's Manual, Version 6.8.

[14] Yu, H., Jeong, D.Y., Gordon, J.E., Tang, Y.H., "Analysis of Impact Energy to Fracture Unnotched Charpy Specimens Made from Railroad Tank Car Steel," Proceedings of the 2007 ASME Rail Transportation Division Fall Technical Conference, RTDF2007-46038, September 2007.

[15] Jeong, D.Y., Yu, H., Gordon, J.E., Tang, Y.H., "Finite Element Analysis of Unnotched Charpy Impact Tests," Materials Science & Technology Conference and Exhibition, 2008.

[16] Yu, H., Tang, Y.H., and Jeong, D.Y., "Elastic-Plastic-Failure Finite Element Analyses of Railroad Tank Car Heads in Impact," Proceedings 2007 ABAQUS Users' Conference, Paris, France, May 2007.

[17] ABAQUS Benchmarks Manual, Version 6.8.

APPENDIX

EXAMPLE PROBLEM

An example problem was developed to test the application of the multi-phase approach and its effectiveness in modeling the FSI effects. The example problem consisted of a one-inch slice of the tank car cross-section (Fig. A1) and was derived from the full-scale tank car model for shell impact Test 2. A lateral pressure load was applied on one side of the tank car slice which was fixed locally on the other side to prevent rigid body motions. The resultant load of the prescribed lateral pressure was denoted as F, and its time history is plotted in Fig. A2. With two distinctive peaks, the shape of the load curve resembled those observed in the shell impact tests. All relevant model parameters were the same as those of the full-scale tank model for Test 2.

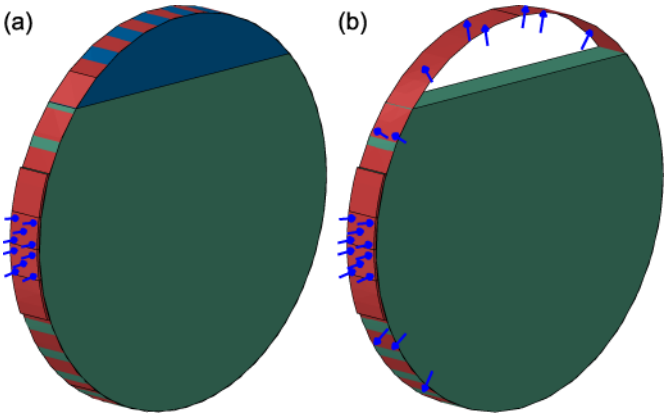

Fig. A1: (a) Multi-phase and (b) simplified FEA models for the example problem

Both the multi-phase and simplified FEA were conducted for the example problem. The multi-phase approach modeled both the liquid and gas phases explicitly and assigned both fluid phases an initial pressure of 100 psi, shown in Fig. A1(a). The simplified approach ignored the gas phase and replaced the fluid pressure with a constant 100 psi imposed on the inner wall of the tank car slice, shown in Fig. A1(b).

The deformation histories obtained from both analyses indicated that (1) the gas phase in the multi-phase model was significantly compressed, and the average gas pressure p_{gas} reached over 350 psi during its time history shown in Fig. A3; (2) the simplified approach predicted unrealistic separations of the solid and fluid surfaces along their interfaces; and (3) compared to the multi-phase FEA, the simplified FEA over-predicted the tank car deformations. The third observation was verified by the F-d curves plotted in Fig. A4, where d was the averaged nodal displacement over the effective load area. The discrepancies between the two model predictions demonstrated that only the multi-phase method fully captured the FSI effects.

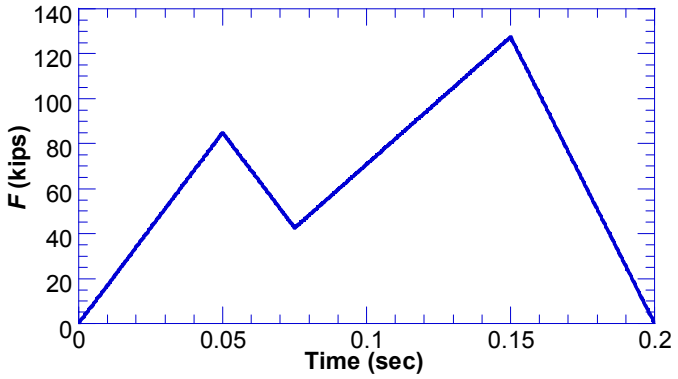

Fig. A2: Time history of the resultant lateral pressure load on one side of the tank car slice

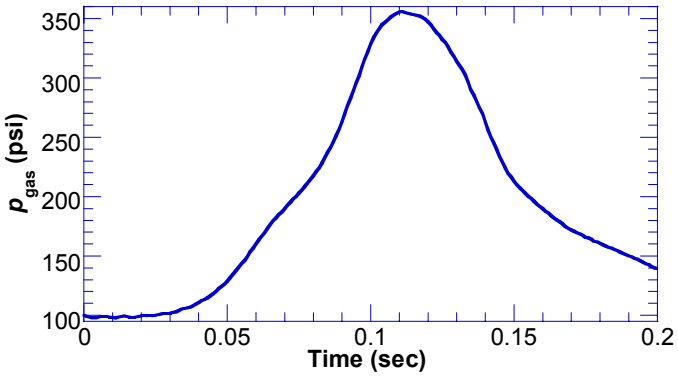

Fig. A3: Time history of the average gas pressure obtained from the multi-phase FEA

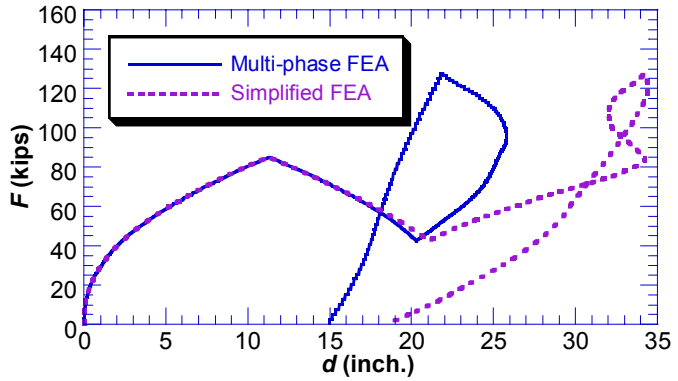

Fig. A4: Comparison of *F-d* curves obtained from multi-phase and simplified FEA